Interplay of impurities and solution flow as determinants of step pattern dynamics

Nicholas A. Booth,[1] Alexander A. Chernov,[2] and Peter G. Vekilov[1]
[1]*Department of Chemical Engineering, University of Houston, Houston, Texas 77204-4004, USA*
[2]*BAE Systems, NASA Marshall Space Flight Center, SD46, Huntsville, Alabama 35812, USA*
(Received 26 August 2003; published 28 January 2004)

The first theory of step pattern evolution, the kinematic wave theory, employed the assumption of impurity effects on step kinetics. On the other hand, recent results have been considered within a framework linking step patterns to the mutual orientation of the solution flow and step motion directions in arbitrarily pure solutions. We explore the consequences of combining impurity and solution flow effects on the dynamics of the surface morphology of the (101) face of potassium dihydrogen phosphate (KDP) crystals. We employ phase-shifting interferometry for real time *in situ* monitoring of these dynamics. We find that, at solution supersaturations $\sigma \leqslant 0.035$, step bunches form on all three vicinals of the (101) face regardless of the mutual orientation of the step motion and solution flow directions. Testing the mechanism of impurity–step pattern interactions, we show that bunching is caused by impurity molecules that adsorb on the surface and slow down and destabilize step trains without inducing growth cessation, i.e., the mechanism is inherently different from the one established for the (100) KDP face. We show that at $\sigma > 0.040$ impurities do not affect step bunching, and it is controlled by the direction of the solution flow, i.e., two distinct regimes of step bunching exist. The transition between the two regimes is governed by the exposure times of the terraces between steps τ: shorter τ's at higher growth rates lead to lower surface concentration of impurities and suppress the impurity effects on step kinetics and bunching.

DOI: 10.1103/PhysRevE.69.011604 PACS number(s): 81.10.−h, 05.65.+b, 68.37.−d, 81.10.Dn

I. INTRODUCTION

Because of the higher surface energy of the crystal-solution interface (higher than, e.g., of the interface between a crystal and its own melt), such interfaces are typically smooth on the atomic or molecular scale and oriented along a low-index crystallographic plane [1]. Correspondingly, their growth proceeds by the generation and spreading of layers. Smooth interfaces experience loss of morphological stability in the form of bunching of the growth steps [2].

Another aspect of the solution growth of crystals is that the presence of impurities is unavoidable, be they unwanted contaminants or intentional additions used to imbue a certain property to the growing crystal. Hence, the first theory of step bunching, the kinematic wave theory, was based on the assumption of impurity effects on step kinetics [3]. Further developments included accounting for time-dependent impurity adsorption, with the surface concentration of impurities on terraces between steps taken as a function of the time of exposure of these terraces, i.e., of the rate of growth [4,5]. There have been numerous experimental works employing a variety of materials in which abundant step bunches, escalating in time and along the steps' pathway, have been attributed to impurity action.

Other studies showed that step bunching in solutions occurs even in arbitrarily pure systems, or with materials and crystallographic faces deemed insensitive to impurity action [6]. A theory was developed linking step bunching to the mutual orientation of the solution flow and step motion directions. It was concluded that if these directions are opposite, equidistant step trains are stable, while confluent directions result in escalating step bunches [7–9].

Many of the investigations of the step bunching instability have been carried out with crystals of potassium dihydrogen phosphate (KDP) or other members of its family [ammonium dihydrogen phosphate (ADP), deuterated KDP (DKDP), and others [10]]. These crystals are grown on a large scale and used as nonlinear optical elements [11] at the National Ignition Facility. There exists a huge information database on these materials [10,12–14] and sources of high-purity salt are available.

The typical habit of the KDP-type crystal consists of prismatic {100} and pyramidal {101} faces. The prismatic faces have a net neutral charge and because of the exposed phosphate residues are particularly susceptible to poisoning by metallic trivalent cations: Cr^{3+}, Fe^{3+}, Al^{3+}, etc. Parts per million amounts of these ions cause two types of deviations from the linear kinetic law of step motion: at lower supersaturations $\sigma < 0.01-0.02$, in the so-called ''dead zone,'' step motion is completely blocked, while in the higher range of $0.02 < \sigma < 0.05$ there is a slow gradual egress to a linear kinetic regime at $\sigma > 0.05$ [15–17]. The initiation of growth as supersaturation is raised above the ''dead zone'' occurs via an elaborate interplay of step bunches and impurity species firmly adsorbed on the terraces [13].

The pyramidal {101} faces are terminated by K^+ ions [18]. As a consequence, the growth of these faces is practically insensitive to the presence of cations, and in many works, this has been the model system for kinetic effects uninhibited by impurities. However, some anions adsorb on {101} surfaces via hydrogen bonds, occupying the positions that otherwise would be taken by the next layer of $H_2PO_4^-$ and greatly inhibit growth, up to inducing a complete growth cessation [19,20]. Similar to the effects of the cationic impurities on the prismatic face, the anions inhibit the kinetics of growth of the pyramidal face at low supersaturations, and may cause complete blocking at higher impurity concentrations.

The goal of this work was to explore if the impurities that slow down growth at lower supersaturations, without completely blocking it, also affect the step bunch patterns. Related issues are whether the impurities affect the response of the expected step bunches to the solution flow direction, and about the transition between impurity-induced and flow-induced instabilities upon supersaturation increase. For these studies, we chose the pyramid, {101} faces of the KDP crystals—because of their lower sensitivity to impurity action the impurity effects do not overwhelm all other features of the growth processes. The onset of instability of equidistant step trains on the {101} KDP faces at supersaturations greater than 0.05, due to interactions of the step pattern with the solution flow, has been addressed in a previous paper [21].

II. EXPERIMENT

A. Phase-shifting interferometry

To visualize *in situ* the growth morphology of crystal surfaces growing from solution we developed a differential phase-shifting interferometer [22]. The device consists of a Michelson interferometer using a He-Ne laser as an illumination source, with a growing crystal face serving as a mirror in one of its arms. To increase the resolution of the technique over traditional interferometry a variable retarder is placed in the reference arm of the interferometer. This allows variations of the optical path length in this arm and hence alters the phase of the reference beam with respect to the contribution from the crystal. We capture a sequence of five images each shifted by $\pi/2$ relative to the previous one and combine them using a standard phase-wrapping algorithm; this gives us a gray scale image coded for height (for details, see [22]).

B. Solutions and crystals

Supersaturated solutions of KDP were prepared and loaded in the crystallization subsystem of the experimental setup as discussed in [22]. After regeneration of the crystal seed at undercooling of $\sim 0.1\,^{\circ}\mathrm{C}$, supersaturation was imposed by lowering the temperature. We evaluate the supersaturation of the solutions as $\sigma=\{CC_e(T)^{-1}-1\}$, with C being the solution concentration, using the solubility dependence on temperature $C_e(T)$, kindly provided by J. J. DeYoreo.

All experiments discussed below used solution flow rates sufficiently fast ($\sim$60 cm/s) to ensure kinetic regime of growth, i.e., the step velocity was independent of flow rate, indicating that growth was controlled by surface kinetics rather than convection and diffusion in the solution bulk.

Figure 1(a) shows a typical phase-wrapped image of a (101) face of KDP. The discontinuities in the gray scale are due to the action of a $\tan^{-1}$ function in the phase-wrapping procedure and are removed during further processing. The image shows the presence of three hillocks that are most likely generated by one or a few screw dislocations outcropping in the central part of the studied face [23]. In a supersaturated solution steps that are generated by a dislocation move with constant linear velocity winding around the dislocation outcrop point [12]. A spiral hillock develops and, after a steady state is reached, covers the whole facet. Due to the anisotropy of the surface kinetics, the hillock has the asymmetric trigonal shape typical of {101} faces of the KDP-ADP class of crystals. The crystal was oriented so that the interference fringes on each of the steep, intermediate, and shallow vicinals were parallel to the corresponding edges of the (101) face. For clarity the image shown in Fig. 1(a) is a close-up of the area surrounding the growth source; this brings the edges of the face outside the field of view. The variation in fringe density over the image highlights the difference in slope of the three vicinal facets typical of this family of crystals.

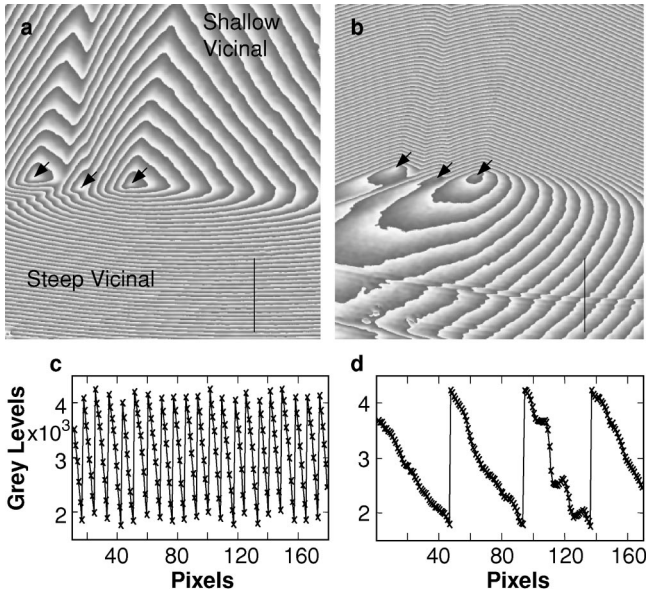

FIG. 1. Optimization of interferometric fringe density used to enhance the resolution of the technique. (a) Phase-shifting interferogram of a correctly aligned (101) face of a KDP crystal (gray levels measure height at pixel location) with the three main vicinal slopes visible. The image does not encompass the whole crystal face—the upper part is truncated by the edge of the field of view. (b) Same image after the crystal has been realigned to decrease the fringe density over the steep facet. (c) and (d) cross profiles taken from the same line as (a) and (b), respectively. In (a) and (b), arrows point at dislocation sources of growth steps.

C. Enhanced characterization of vicinal morphology

The slope of the steep vicinal is approximately 5$\times$ greater than that of the shallow vicinal. The associated high density of interferometric fringes on the steep vicinal leads to a fringe width of 5–10 pixels, Fig. 1(c). Such narrow fringes lead to a reduction in the depth and lateral resolution of the imaging. Indeed, each phase-wrapped fringe encompasses 0.113 μm of height, and with an average fringe width of 8 pixels, as in Figs. 1(a) and 1(c), the depth resolution is limited to 0.014 μm.

To increase the resolution of the data for the steep vicinal we realign the crystal in such a way as to lower the fringe density [see Fig. 1(b)]. Since we use a camera with a 12-bit encoding of the gray color intensity, a pixel density of 4096

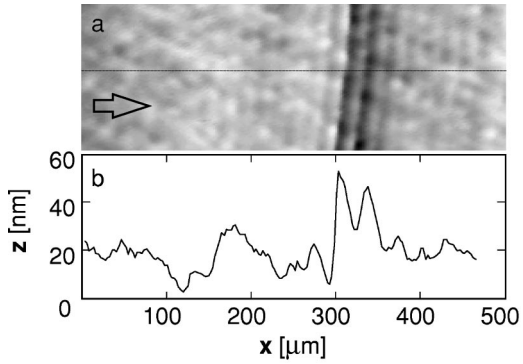

FIG. 2. A typical step bunch on KDP (101). (a) Differential phase-shifting image; (b) cross section along line in the middle of (a). Solution flow direction is indicated by the arrow. Steps move in the same direction.

per fringe would theoretically yield a resolution of 0.03 nm. However, the interferometric technique compares the deviations from flatness of the crystal surface with the flatness of a reference mirror. Hence, the resolution is limited by the roughness of this reference surface. In our case the reference surface is certifiably flat to (1/60) λ (the laser wavelength $\lambda = 633$ nm) over the ~ 1 cm^2 of the surface of the reference mirror. We found that over the area less than 1 mm^2 that we image interferometrically, the deviation from surface flatness is about half of that, i.e., the resolution limit is about ± 2.5 nm [22].

To quantify the heights of observed step patterns, we use the ratio of the fringe densities before and after realignment as a scaling factor. Figure 1(b) shows a typical case, in which upon realignment we obtain a fringe density of approximately 50 pixels per fringe. Figure 1(d) illustrates how the achieved increase in resolution reveals several small step bunches—note the distortion of the fringes in the lower part of Figs. 1(b) and 1(d).

Figure 2 shows an unwrapped differential image of the surface and a cross section of the step bunch profile that highlight the local morphology [22]. The cross section Fig. 2(b) reveals a pair of step bunches approximately 40 nm high. Additional surface features are revealed by the area image in Fig. 2(a). The area image can be viewed as a combination of a number of parallel surface profiles as the one in Fig. 2(b), with the surface height encoded as a gray intensity level. We see in Fig. 2(a) that ~ 10–12 smaller bunches parallel to the main pair exist. Since the interference fringes are roughly perpendicular to step bunches, these smaller features are likely not interference artifacts. We conclude that these are smaller step bunches of height ~ 5 nm and higher, detectable over the mottled background due to the reference mirror roughness because of their parallel mutual orientation.

To obtain representative characteristics of the step bunch height under certain conditions, we remove noise in the image due to the roughness of the reference surface. For this, we select an area of interest and extract five parallel surface profiles, separated by 2–3 pixels; see Fig. 3(a). We combine the five profiles and obtain the average shown in Fig. 3(b). Since one pixel corresponds to $\sim 2 \times 2$ μm^2 of the crystal surface area, the width over which the profiles are collected is ~ 25 μm. An average step bunch height H was calculated as the average of the Δz's between the minima and their two adjacent maxima in Fig. 3(b).

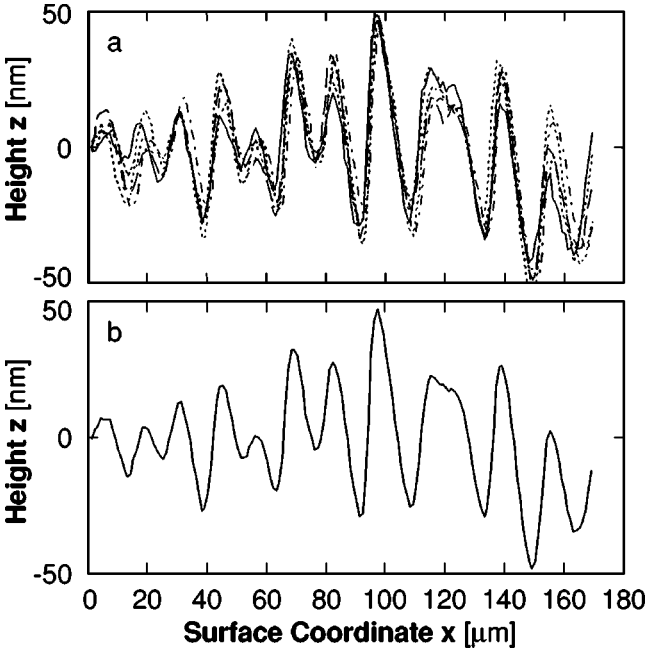

FIG. 3. Quantification of step bunch height. (a) Shows five parallel cross sections of the same step bunch profile, each separated from its near neighbor by ~ 2 μm laterally. The five profiles are used to form an average, shown in (b), which removes random and short-range noise from the trace.

III. RESULTS AND DISCUSSION

A. Step bunching at low supersaturations

Previous experiments, typically carried out at $\sigma \geqslant 0.05$ [24] have shown that the direction of solution flow over a surface with respect to that of step motion can have either a stabilizing or destabilizing effect regarding the formation of step bunches. They show that step bunches form only on the vicinals where the directions of step propagation and solution flow coincide. Reversing the direction of solution flow has the effect of removing existing bunches and leads to the formation of new ones on other vicinals that have step motion in the same direction as the new solution flow. A theoretical explanation of the coupling of solution flow and step bunching is provided in Refs. [7–9,25].

Figure 4(a) shows a (101) face of KDP containing two dislocation growth sources. The two growth hillocks generated by these sources have their shallow vicinals to their left and intermediate vicinals to the right; the steep vicinal of the lower hillock vertically separates the two sources. Previous work [7,26] suggests that if the solution flow direction is as in Fig. 4(a) the shallow and intermediate vicinals are in a stabilizing regime because of the largely antiparallel directions of solution flow and step motion. Similarly, on the steep vicinal where step motion is parallel to the solution flow step train destabilization and step bunching is expected. However,

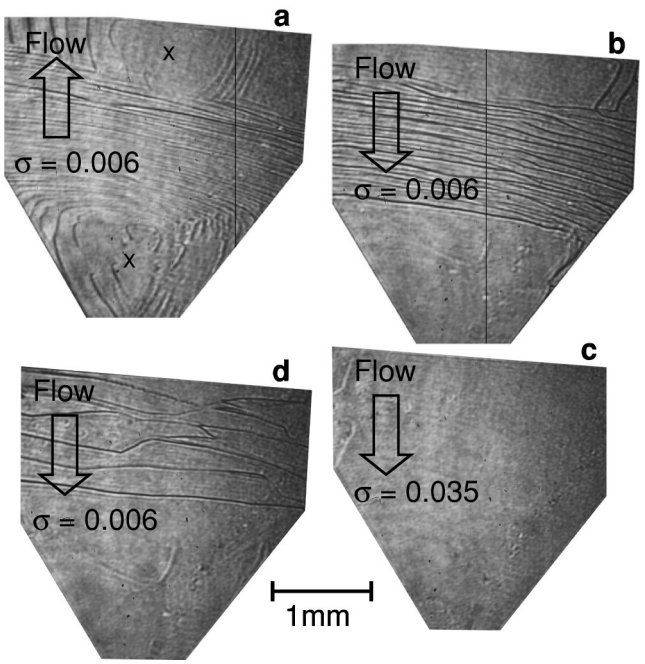

FIG. 4. The effect of flow direction and supersaturation σ on step bunch formation. Single-beam images of the (101) face. The value of σ is displayed and the direction of solution flow indicated by an arrow in each panel. The time between sequential images is approximately 10 min. To the left and right of each source are, respectively, shallow and intermediate vicinals. Only one steep vicinal, originating from the lower source is seen. In (a) the location of two dislocation step sources are marked with $\times$. Step bunches are visible over the entire (101) face but are most pronounced on the shallow and intermediate vicinals. (b) The surface morphology after the direction of solution flow was reversed. The degree of step bunching on the steep vicinal is now much more pronounced while on the shallow and intermediate vicinals bunching is almost eliminated. (c) Illustrates the effect of increasing σ to 0.035—step bunches are now almost entirely absent over the whole (101) face. After reducing σ back to 0.006 step bunches again form on the steep vicinal in (d).

Fig. 4(a) shows that this is not the case—in addition to bunches on the steep vicinal, strong bunching also occurs on the shallow and intermediate vicinals.

After a reversal of the direction of solution flow, the step bunch pattern changed to that in Fig. 4(b). Bunching is now almost exclusively confined to the steep vicinal where the direction of solution flow is against that of step motion, and this is again contrary to expectations based on the previous results at $\sigma > 0.05$. When σ was increased from 0.006 to 0.035, the bunches on the steep vicinal were eliminated [Fig. 4(c)]. With a further increase of σ to greater than 0.035, bunches eventually formed on the shallow and intermediate vicinals (image not shown) that were now in a destabilizing flow regime. Lowering σ back to below 0.01 caused the step bunches to again form on the steep vicinal [Fig. 4(d)]. The changes in the surface morphology, illustrated by the cycle in Fig. 4, take place over a period of 5–10 min after the respective change in the growth conditions either in the direction shown in Fig. 4, or in the reverse. Other similar sequences of data collected at both possible directions of solution flow and

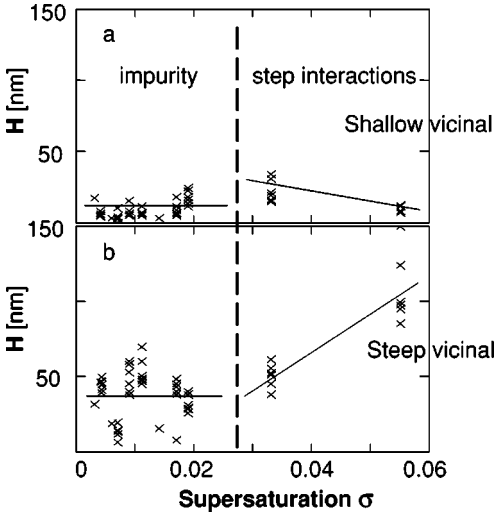

FIG. 5. Dependence on the supersaturation σ of the average step bunch height H of representative profiles on the shallow and steep vicinals. In all determinations, the solution flow direction was as in Fig. 4(a), i.e., along the step motion direction on the steep vicinal and opposite the step motion direction in the shallow vicinal.

at variable supersaturation in the range 0.05–0.07 revealed that, as in Fig. 4, at lower σ's step bunches are present on all vicinals, while at higher σ's, step bunches are detectable only on the step trains traveling in the direction of the solution flow.

The significant features of the step bunches monitored in Fig. 4 and in numerous similar sequences are as follows. (i) Their dynamic behavior—strong bunches split into lower-height formations which reform into new bunches. The average lifetime of a bunch is 30–60 s. (ii) The limited step bunch height—as bunches propagate down the steps' pathway, their height does not increase indefinitely, but a limiting value is reached. In a parallel investigation (in preparation) we show that the constrained step bunch evolution is due to the step bunch dynamics and correlate them to the high turbulence of the solution flow.

B. The two step bunching regimes

The response of average bunch height H on the two vicinals to σ variations with the solution flow directed opposite the step motion direction on the shallow vicinal—as in Fig. 4(a)—is shown in Fig. 5. The average H on the shallow vicinal in Fig. 5(a), between 5 and 30 nm (this range is above the resolution limit of the interferometer of 5 nm), is significantly lower than H on the steep vicinal in Fig. 5(b) across the full range of σ. The lower H's on the shallow vicinal are likely due to its lower slope—slope has been identified as a major destabilizing factor for step trains [7,9]. The data in Fig. 5(a) split into two. Below $\sigma \approx 0.035$, where visible step bunches are present in images such as those in Fig. 4(a) on the shallow vicinal, the average bunch height increases as higher supersaturations. At $\sigma > 0.040$, the step bunch height on the shallow vicinal is lower than in the lower σ range, and no step bunches are detectable. As discussed in relation to Fig. 4, upon changing of σ from a value in one range to a

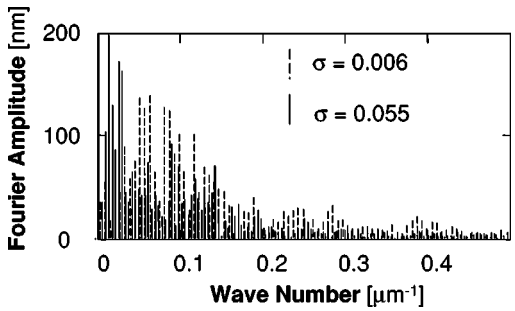

FIG. 6. Fourier transforms of two step patterns taken at $\sigma = 0.006$ and $\sigma = 0.055$, respectively, i.e., in impurity-induced and flow-induced instability regimes.

value into the other, the step bunch patterns typical of the new regime ensue within ~5–10 min. We conclude that two distinct step bunching mechanisms act at $\sigma < 0.04$, and at $\sigma > 0.04$. In the low supersaturation range, bunching is caused by impurity molecules that adsorb on the surface and slow down and destabilize step trains without inducing growth cessation. At high supersaturations, the classical mechanism of solution flow—the step pattern interaction, discussed above, operates.

The existence of two different step bunching mechanisms is supported by the Fourier transforms of two surface profiles, taken from the steep vicinal at $\sigma = 0.006$ and $\sigma = 0.055$, i.e., in the low and high supersaturation ranges, shown in Fig. 6. For $\sigma = 0.055$ we see large Fourier amplitudes at low wave numbers whereas at $\sigma = 0.006$ the Fourier amplitudes are generally lower and more uniformly spread over larger wave numbers. Thus, in the lower supersaturation range, the spectra of the step bunching instability shift to higher wave numbers (shorter wavelengths) and lower amplitudes.

C. Impurity action on the (101) KDP face

In the context of the low growth rates occurring at low σ's, we invoke impurity action as the cause of the unusual step bunching. Indeed, at low growth rates R, the exposure times of the terraces between steps $\tau = h/R$ [h is the step height = 5.1 Å for the (101) KDP face [10]] are longer. This allows for a higher surface concentration of impurity species, the characteristic adsorption times of which are comparable to the terrace exposure times [3,5,10].

Since no impurities were intentionally added to the growth solution, we assign the postulated impurity effects to the uncontrolled impurities present in the salt and those released from the materials of the crystallization apparatus. The compositional analysis of the KDP salt used in this experiments indicates that the amounts of trivalent transition metal and ~40 other inorganic ions are below the detection limits of the analytical techniques employed, 50–200 ppb [27]. However, the sensitivity of the techniques used to detect organic species is typically significantly lower. Furthermore, while the crystallization cell and the tubing are made of Teflon and Tygon, respectively, which are considered unlikely sources of contamination, the crystallization container is built of polyethylene [22], known to release trace amounts

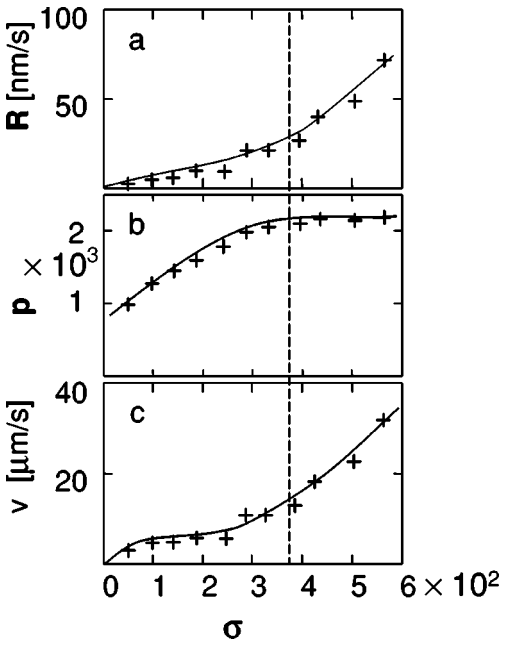

FIG. 7. Dependencies of the normal growth rate R, vicinal slope p, and step velocity v, on the supersaturation σ. The p and v dependencies are for the shallow vicinal. Curves are just guides for the eye.

of hydrocarbons into the solution. Thus, it is likely that organic impurities at concentrations below the detection limits of the spectroscopic techniques available to us are present in the growth solution. It has been shown that organic impurities affect the kinetics of step propagation on the (101) KDP face [19,20] and that the impurity effects are stronger at low supersaturations [20]. The latter result, obtained with KDP material similar to the one that we use, suggests that the characteristic adsorption times of the uncontrolled organic impurities are comparable to the terrace exposure times at low supersaturations [20].

D. The supersaturation dependence of the average step velocity

For independent evidence of impurity action on the growth processes, we monitored the kinetics of crystal growth, averaged over periods of 10–20 min. The dependencies of the normal growth rate and the vicinal slope in Figs. 7(a) and 7(b) are typical for many solution growth systems and do not allow any conclusions about factors that might be affecting the growth kinetics. However, the superlinear dependence of the step velocity ν on σ deviates from the typical linear or sublinear laws [28,29].

Superlinear $\nu(\sigma)$ dependencies have been attributed to two mechanisms. (i) If the kink density at lower σ's is ''low'' so that diffusion of material along the step to a kink is a rate limiting factor, increasing kink density with higher supersaturation leads to a stronger than linear increase in ν [30]. (ii) The action of one or more impurity species, the characteristic adsorption times of which are comparable to the terrace exposure times τ. Thus, higher supersaturations, higher R's, and lower τ's result in lower surface concentration of

impurities and faster ν's. A self-consistent analytical derivation has shown that this scenario leads to a superlinear $\nu(\sigma)$ [17,31].

Low kink density on a (101) KDP face is unlikely. The kink density in equilibrium and at low supersaturations is determined by the intermolecular bond energy in the crystal. Based on similarity in crystallization enthalpy, the energy of the intermolecular bonds in KDP crystals is similar to the one in ammonium dihydrogen phosphate crystals [10]. No superlinear step kinetic laws suggestive of low step density have been observed with ADP [28]. This conclusion is supported by high-resolution atomic force microscopy images of the steps on the (101) KDP face showing very rough steps [12,32].

Thus, we interpret the observed superlinear shape of the $\nu(\sigma)$ dependence as evidence for impurity effects on the step kinetics. As discussed above, the likely impurities that affect the growth kinetics and the step bunching patterns at low supersaturations are organic species present in the KDP material or released by the polyethylene solution container, rather than trivalent or other inorganic cations.

E. Comparison with the (100) KDP face

The growth kinetics of the (100) KDP face are strongly affected by trivalent transition metal ions, which adsorb on the crystal surface and delay and completely block growth at $\sigma < 0.035$, in the ''dead zone'' [10,16]. Quite unexpectedly, it was shown that the impurity action and the response of the growth kinetics strongly deviate from the predictions of a classical theory of closely spaced impurity stoppers [33], and even of its later modifications [17,31]. It was shown that ''supersteps''—stable accumulations of numerous elementary steps—are an important part of the mechanisms of growth cessation and resumption upon changing of σ in and out of the dead zone [13]. Thus, growth was shown to resume only after a ''superstep'' ''sweeps'' the surface ''clean'' of adsorbed impurities [13].

Although we have shown above that the growth mechanism on the (101) KDP face at low supersaturations has many elements of the kinetics observed on the (100) face, there are significant differences. (i) The maximum step density within bunches in Figs. 2 and 3 is at most (3–4) times higher than average step density on the vicinal, and (ii) the step bunches are dynamic entities that form and decay with a mean lifetime of 30–60 s. Thus, these step bunches differ significantly from the ''supersteps'' present on the (100) face [13]. (iii) There is no ''dead zone'' on the (101) face, and growth proceeds even at the lowest supersaturations. We conclude that the mechanism of impurity–step bunch interplay on the (101) face is more akin to those assumed by the classical models [3,5], whereby the impurity species affect step propagation and enhance step bunching, with the magnitude of these effects dependent on the supersaturation via the growth rate and the terrace exposure times.

ACKNOWLEDGMENTS

We thank J. J. DeYoreo and T. Land for generously providing ultrapure KDP salt. This work was supported by the Office of Biological and Physical Research, NASA, under Grant No. NAG8-1454.

[1] I. V. Markov, *Crystal Growth for Beginners. Foundations of Nucleation, Crystal Growth and Epitaxy* (World Scientific, Singapore, 1995).
[2] *A Schematic Mechanism for Striated Growth of Solid Binary Mixtures*, edited by B. Caroli, C. Caroli, and B. Roulet (Cambridge University Press, Cambridge, England, 1992).
[3] F. C. Frank, in *Growth and Perfection of Crystals*, edited by R. H. Doremus, B. W. Roberts, and D. Turnbul (Wiley, New York, 1958), p. 411.
[4] J. P. Van der Eerden and H. Mueller-Krumbhaar, Phys. Rev. Lett. **57**, 2431 (1986).
[5] J. P. Van der Eerden and H. Mueller-Krumbhaar, Electrochim. Acta **31**, 1007 (1986); A. A. Chernov, V. F. Parvov, M. O. Kliya, D. V. Kostomarov, and Y. G. Kuznetsov, Sov. Phys. Crystallogr. **26**, 640 (1981).
[6] A. A. Chernov, Y. G. Kuznetsov, I. L. Smol'sky, and V. N. Rozhanskii, Sov. Phys. Crystallogr. **31**, 705 (1986).
[7] A. A. Chernov, J. Cryst. Growth **118**, 333 (1992).
[8] A. A. Chernov, S. R. Coriell, and B. T. Murray, J. Cryst. Growth **132**, 405 (1993).
[9] S. R. Coriell, B. T. Murrary, A. A. Chernov, and G. B. McFadden, J. Cryst. Growth **169**, 773 (1996).
[10] L. N. Rashkovich, *KDP-Family Single Crystals* (Adam Hilger, Bristol, 1991).
[11] M. H. Key, Nature (London) **412**, 775 (2001).
[12] J. J. DeYoreo, T. A. Land, and B. Dair, Phys. Rev. Lett. **73**, 838 (1994).
[13] T. A. Land, T. L. Martin, S. Potapenko, G. T. Palmore, and J. J. De Yoreo, Nature (London) **399**, 442 (1999).
[14] N. Zaitseva and L. Carman, Prog. Cryst. Growth Charact. Mater. **43**, 1 (2001).
[15] L. N. Rashkovich, A. A. Mkrtchan, and A. A. Chernov, Sov. Phys. Crystallogr. **30**, 350 (1985); L. N. Rashkovich, N. V. Gvozdev, and I. V. Yamlinski, Crystallogr. Rep. **43**, 669 (1998).
[16] L. N. Rashkovich and B. Y. Shekunov, J. Cryst. Growth **100**, 133 (1990).
[17] V. V. Voronkov and L. N. Rashkovich, J. Cryst. Growth **144**, 107 (1994).
[18] S. A. de Vries, P. Goedtkindt, S. L. Bennett, W. J. Huisman, M. J. Zwanenburg, D.-M. Smilgies, J. J. De Yoreo, W. J. P. van Enckevort, P. Bennema, and E. Vlieg, Phys. Rev. Lett. **80**, 2229 (1998).
[19] Y.-J. Fu, Z.-S. Gao, J.-M. Liu, Y.-P. Li, H. Zeng, and M.-H. Jiang, J. Cryst. Growth **198/199**, 682 (1999).
[20] O. Gliko, N. P. Zaitseva, and L. N. Rashkovich, in *Morphology and Dynamics of Crystal Surfaces in Complex Molecular Systems*, edited by J. DeYoreo, W. Casey, A. Malkin, E. Vlieg, and M. Ward, Mater. Res. Soc. Symp. Proc. No. 620 (Materials Research Society, Pittsburgh, 2001).

[21] N. A. Booth, A. A. Chernov, and P. G. Vekilov, J. Cryst. Growth **237–239**, 1818 (2002).
[22] N. A. Booth, B. Stanojev, A. A. Chernov, and P. G. Vekilov, Rev. Sci. Instrum. **73**, 3540 (2002).
[23] Y. G. Kuznetsov, A. A. Chernov, P. G. Vekilov, and I. L. Smol'skii, Sov. Phys. Crystallogr. **32**, 584 (1987).
[24] A. A. Chernov, L. N. Rashkovich, and A. A. Mkrtchan, J. Cryst. Growth **74**, 101 (1986).
[25] S. R. Coriell, A. A. Chernov, B. T. Murray, and G. B. McFadden, J. Cryst. Growth **183**, 669 (1998).
[26] W. J. P. van Enckevort, Prog. Cryst. Growth Charact. **9**, 1 (1984).
[27] N. Zaitseva, L. Carman, I. Smolsky, R. Torres, and M. Yan, J. Cryst. Growth **204**, 512 (1999).
[28] P. G. Vekilov, Y. G. Kuznetsov, and A. A. Chernov, J. Cryst. Growth **121**, 643 (1992).
[29] K. Maiwa, K. Tsukamoto, and I. Sunagawa, J. Cryst. Growth **102**, 43 (1990); K. Onuma, T. Kameyama, and K. Tsukamoto, *ibid.* **137**, 610 (1994); T. A. Land, J. J. DeYoreo, and J. D. Lee, Surf. Sci. **384**, 136 (1997); D. N. Petsev, K. Chen, O. Gliko, and P. G. Vekilov, Proc. Natl. Acad. Sci. U.S.A. **100**, 792 (2003).
[30] H. H. Teng, P. M. Dove, C. A. Orme, and J. J. De Yoreo, Science **282**, 724 (1998); K. J. Davis, P. M. Dove, and J. J. D. Yoreo, *ibid.* **290**, 1134 (2000).
[31] V. V. Voronkov and L. N. Rashkovich, Sov. Phys. Crystallogr. **37**, 289 (1992).
[32] T. A. Land, J. J. De Yoreo, T. L. Martin, and G. T. Palmore, Crystallogr. Rep. **44**, 655 (1999).
[33] N. Cabrera and D. A. Vermileya, in *Growth and Perfection of Crystals*, edited by R. H. Doremus, B. W. Roberts, and D. Turnbul (Wiley, New York, 1958).